IMPACT TENSION PROPERTIES IN A2091 ALUMINUM-LITHIUM ALLOY

Akihiro Takahashi, Toshiro Kobayashi and Hiroyuki Toda

Department of Production Systems Engineering,
Toyohashi University of Technology, Tempaku-cho, Toyohashi, AICHI 441-8580 Japan

ABSTRUCT

The impact tension behavior of 2091 aluminum alloy is investigated over a wide range of strain rates(1.0×10^{-6} to 830 s^{-1}) at room temperature. Yield and ultimate tensile strength increase with increasing strain rate. Fracture surface exhibits shear fracture with extensive delamination cracking, and is remarkably rough at high strain rates. The microcracks which are initiated at second phase particles are observed and quantified.

Keywords: *A2091 Aluminum-Lithium alloy, impact tension test, strain rate dependency, microcrack,*

1. INTRODUCTION

Over the past decade, Al-Li alloys have received significant attention for stiff structures due to their low density and high Young's modulus, which is 10 to 15 pct higher than the other commercial aluminum alloys. [1] For the airframe applications, therefore, reduction of density concomitant with increases in elastic modulus and strengthening in yield stress leads to improvement of strength-to-weight ratio. The alloys have inspired a wide range of research activities, such the strength, fracture toughness and fatigue resistance, in order to improve the properties.

For Environmental problems, recently, the applications of aluminum alloys for automobile instead of ferrous materials are becoming an attractive topic in automobile industry. [2] While, the majority of reports on the mechanical properties are concentrated on the properties in Charpy tests or dynamic fracture toughness tests. [3-5] The stress-strain curves under the high strain rate are required to analyze various traffic accidents and to design automobile bodies using computer simulations. Thus, the measurement of stress-strain curves at high strain rates is important.

The objective of the present study is to establish the measuring method of stress-strain curves and to investigate the impact tensile behavior of Al-Li alloy up to 830 s^{-1}. To clear damages on failure, the fracture surfaces and the longitudinal section area of broken specimens are observed and quantified.

2. EXPERIMENTAL PROCEDURES

2.1 Material

The material used in the present work is an A2091 Al-Li alloy. The chemical composition are given in Table 1 of these, Fe and Si are major impurities. The as-received plate having thickness of 22mm had been cast, homogenized, warm rolled, and annealed. The plate was then solution treated

at 793 K in a salt bath for 1 hour, qenched in water, cold rolled and aged at 433 K in oil bath for 24 hours. The microstructure is shown in Fig. 1.

Table 1 Chemical composition (mass%)

Li	Cu	Mg	Zr	Fe	Si	Al
2.1	2.0	1.5	0.12	<0.06	<0.03	bal.

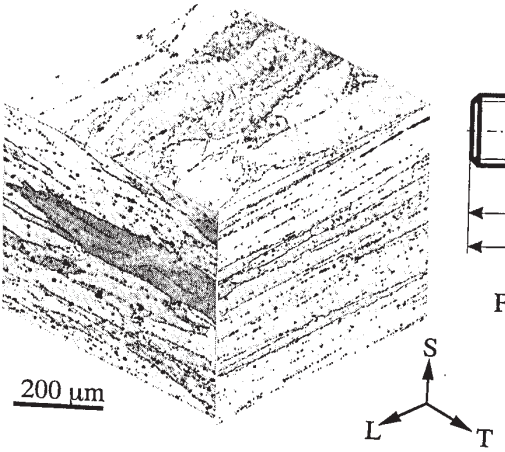

Fig. 1 Optical microstructure.

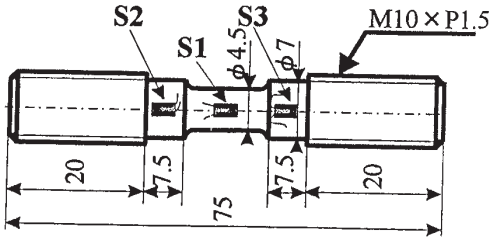

Fig.2 Schematic illustration of the tensile specimen and the location of strain gages. (in mm)

2.2 Tensile test

The specimen was machined from the plate with parallel to the prior rolling direction on loading axis, which has shoulders parallel to the gage section as shown in Fig. 2. Three strain gages were glued on the three sections, respectively. The strain gage in the gage length (S1) was used for strain measurement while S2 and S3 on the shoulders were used for the measurement of applied to the specimen. Before the Impact tension tests the static tensile tests were performed using Instron tensile testing machine(5583 type) and calibration values for S2 and S3 were also obtained. The Impact tension tests were carried out using a hydraulic impact tension testing machine(EHF-U5H-20L type, Shimazu Corp.).[6]

Loading velocity was varied from 8.3×10^{-6} to 10m/s(corresponding strain rate was 1×10^{-6} to $830s^{-1}$).

2.3 SEM observation

Fracture surfaces of the fractured specimens were observed with a scanning electron microscope (JSM-6300, JEOL Ltd.). In the longitudinal section of the broken specimens, extensive delamination crackings and microcracks which were originated from second phase particles were also observed with the SEM to examine the feature of a damage zone.

3. RESULTS AND DISCUSSION

3.1 Stress-strain curve under impact loading

Figure 3 shows the load-time curves obtained from the impact tests conducted under 3m/s (205 s^{-1}).

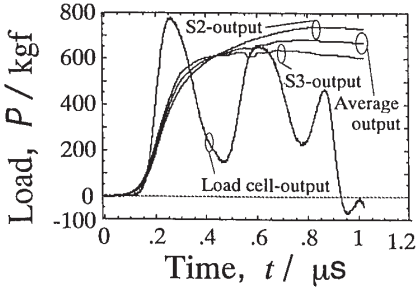

Fig. 3 Load-time curves.

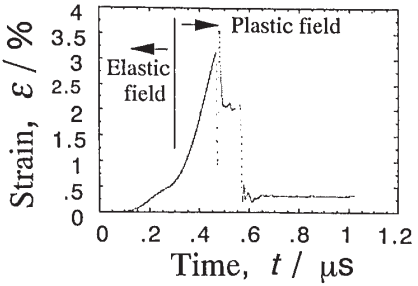

Fig. 4 Strain-time curve.

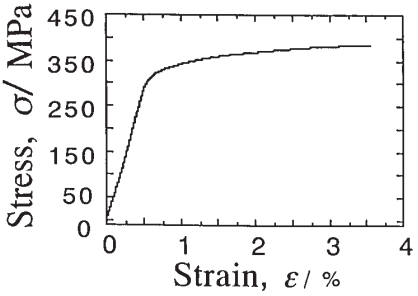

Fig. 5 Stress-strain curve.

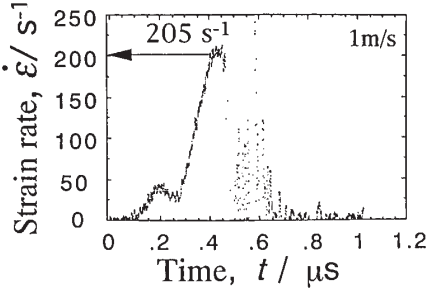

Fig. 6 Strain rate-time curve.

In the Fig. 3, there are four load signals which are the load cell output obtained from impact testing machine, the strain gage(S2 and S3) outputs and the average of S2 output and S3 output attached on the specimen. It can be found that the form of load cell output-time curve is shaken violently relatively at high strain rates. Therefore, it is difficult to estimate mechanical properties of the material, such as the yield strength and ultimate tensile strength, with load cell output-time curve. While, though the S2 strain gage output-time curve is different from the S3 curve, it could be considered that the deformation behavior of the specimen is exactly described to both of the strain gage curves. In this study, the average of S2 and S3 output is adopted as load-time curves in the material.

Figure 4 shows the strain-time curve obtained from the tests conducted under the $205s^{-1}$. Fig. 5 is the stress-strain curve which is deduced from the data in Fig. 3 and Fig. 4. In the Fig. 6, The definition of strain rates is indicated. The strain rate data on the vertical axis is differentiated from the strain data from S1 output.

3.2 Tensile properties

The mechanical properties of the tested A2091 alloy were summarized in Fig. 7. Figures 7a and 7b show the change of tensile strength with strain rate, as well as the change of elongation to failure and reduction of area. In both Figures, yield strength, elongation and reduction of area increase with increasing strain rate. The elongation to failure is measured by matching the fracture

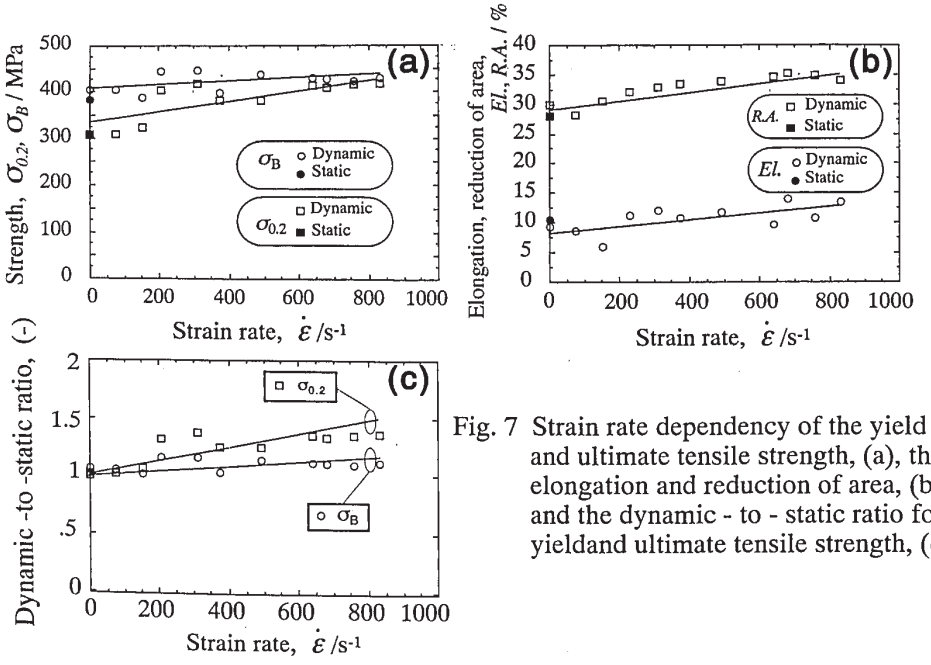

Fig. 7 Strain rate dependency of the yield and ultimate tensile strength, (a), the elongation and reduction of area, (b), and the dynamic - to - static ratio for yieldand ultimate tensile strength, (c).

surfaces. Figure 7c shows the strain rate dependency of dynamic – to – static ratio for yield and ultimate tensile strength, where the dynamic – to – static ratio is defined as a strength value at each strain rate normalized by that in the static condition. Yield strength is more sensitive to strain rate than ultimate tensile strength.

3.3 Fracture surfaces

Fracture surfaces obtained at various strain rate are shown in Fig. 8. Fracture surfaces of all the specimens exhibit shear fracture with extensive delamination cracking, fracture surface roughness increases with increasing strain rate.

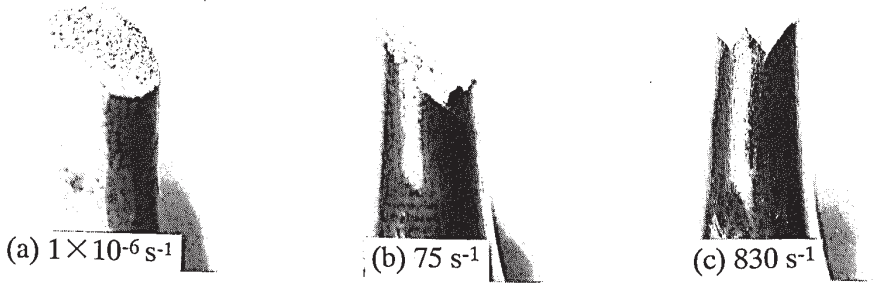

Fig. 8 Fracture surfaces obtained at strain rate of 1×10^{-6}s^{-1},(a), 75 s^{-1},(b), and 830 s^{-1},(c).

Figure 9 shows SEM fractographs of the fractured specimens. Fracture surface of the specimen tested at 1.0×10^{-6} s^{-1} is very smooth and flat, while those tested at 75 and 830s^{-1} shows freqent crack diffection.

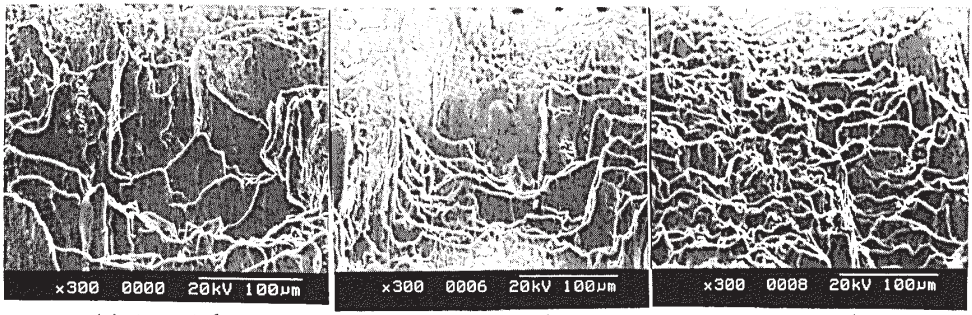

(a) $1\times10^{-6}s^{-1}$ (b) 75 s^{-1} (c) 830 s^{-1}

Fig. 9 SEM fractographs of the fractured specimens obtained at strain rate of $1\times10^{-6}s^{-1}$,(a), 75 s^{-1},(b), and 830 s^{-1},(c).

3.4 Delamination cracking and microcracks

Figure 10 shows the longitudinal section of a broken specimen tested at strain rate of 830s^{-1}. In Fig. 10, the extensive delamination crackings are observed. The crack passes along grain boundaries and sub-grain boundaries parallel to the tensile axis, in which they are linked by shear deformation. The tendency of grain boundary failure in Al-Li alloys has been attributed to planer slip, strain localization in PFZ, grain boundary embrittlement due to the precipitation of δ'(Al_3Li phase). Figures 11a and 11b are hystograms which show number of featured second phase particles and that of remaining particles or specimen surface after impact tension tested at strain rate of 830s^{-1}. Second phase particle size is defined as shown Fig. 11c. Quantitative measurements for number of fractured second phase particles and that of remaining particles were made from the longitudinal section beneath gage length on specimens. Hence, the damage zone extends over a wide area at high strain rate when tested.The crack density is higher with increasing strain rate, therefore, it is thought that the damage zone and level of high strain rate tested specimens is larger than low strain rate specimens.

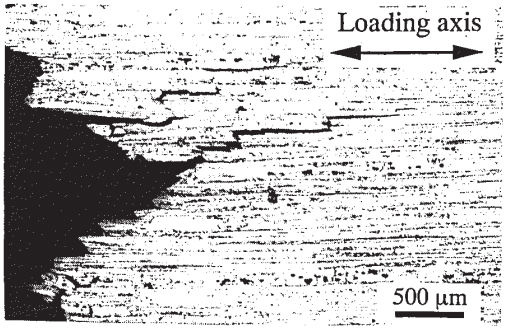

Fig. 10 The longitudinal section of a broken specimen tested at strain rate of 830 s^{-1}.

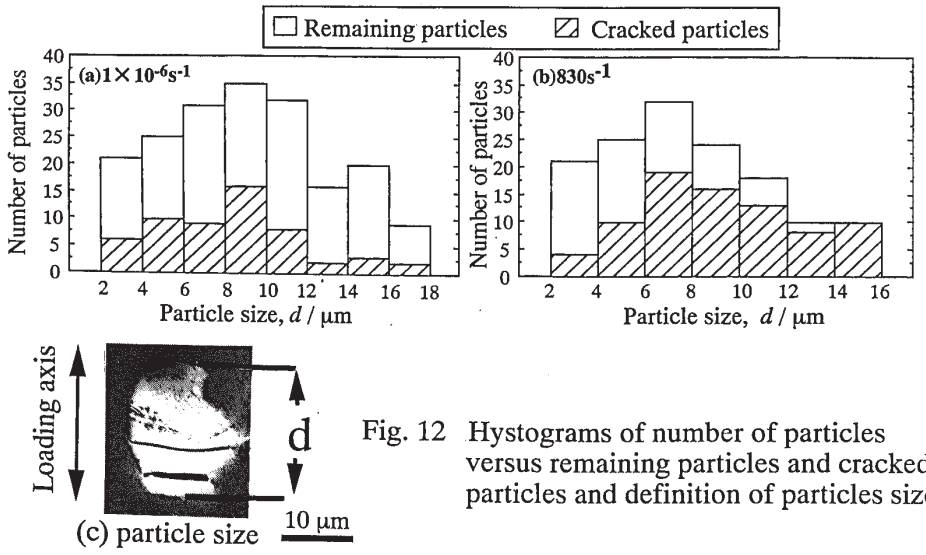

Fig. 12 Hystograms of number of particles versus remaining particles and cracked particles and definition of particles size.

4. CONCLUSIONS

Impact tension tests at strain rates up to $830s^{-1}$ were carried out in an A2091 aluminum-lithium alloy. The results and conclusions are summarized as follows.

(1)The impact tension load can be more exactly measured by measuring load level two strain gages attached on the sholders of a specimen.

(2)The yield strength, elongation to failure and reduction of area increases with increasing strain rates up to $830s^{-1}$.

(3)Fracture surface exhibit the features of shear fracture at all of the strain rate with extensive delamination cracking.

(4) The damage zone extends over a wide area when tested at high strain rate.

REFERENCES

[1] B. Noble, S. J. Harris, K. Dinsdale : J. Mater. Sci, 17(1982), 461.

[2] T. Moons, P. Ratchev, P. De Smet, B. Verlinden and P. Van Houtte : Scripta Metar, 35(1996), 939.

[3] T. Kobayashi, M. Niinimi and K. Degawa : J. Jpn. Inst. Metals, 52(1988), 34.

[4] T. Kobayashi, M. Niinimi and I. Kanoya : J. Jpn. Inst. Light Metals, 43(1993), 95.

[5] N. E. Prasad, S. V. Kamat, G. Malakondaiah and V. V. Kutumbarao : Fatigue Fract. Engng. Mater. Struct, 17(1994), 441.

[6] T. Kobayashi and I. Yamamoto : Proc. ICAA-5, Part 3(1996), 1383.